



PCCP

Energetics and Kinetics of Various Cyano Radical Hydrogen Abstractions

Journal:	<i>Physical Chemistry Chemical Physics</i>
Manuscript ID	CP-ART-12-2020-006228.R1
Article Type:	Paper
Date Submitted by the Author:	19-Jan-2021
Complete List of Authors:	Burke, Alexandra; University of Georgia Franklin College of Arts and Sciences, Center for Computational Quantum Chemistry Bowman, Michael; Taylor University, Department of Chemistry and Biochemistry Turney, Justin; University of Georgia, Center for Computational Quantum Chemistry Schaefer, Henry; University of Georgia, Computational Chemistry

SCHOLARONE™
Manuscripts

Cite this: DOI: 00.0000/xxxxxxxxxx

Energetics and Kinetics of Various Cyano Radical Hydrogen Abstractions[†]

Alexandra D. Burke,^a Michael C. Bowman,^b Justin M. Turney,^a and Henry F. Schaefer III^{*a}

Received Date

Accepted Date

DOI: 00.0000/xxxxxxxxxx

The cyano radical (CN) is an abundant, open-shell molecule found in a variety of environments, including the atmosphere, the interstellar medium and combustion processes. In these environments, it often reacts with small, closed-shell molecules via hydrogen abstraction. Both carbon and nitrogen atoms of the cyano radical are reactive sites, however the carbon is more reactive with reaction barrier heights generally between 2-15 kcal mol⁻¹ lower than those of the analogous nitrogen. The CN + HX → HCN/HNC + X, with X=H, CH₃, NH₂, OH, F, SiH₃, PH₂, SH, Cl, C₂H, CN reactions have been studied at a high-level of theory, including CCSD(T)-F12a. Furthermore, kinetics were obtained over the 100-1000 K temperature range, showing excellent agreement with those rate constants that have been determined experimentally.

1 Introduction

In addition to being one of the first radicals to be detected in the interstellar medium (ISM), the cyano radical (CN) is also one of the most abundant open-shell molecules found in the ISM.^{1,2} The CN radical has been identified in Titan's atmosphere³ as well as the atmospheres of the outer planets and some of their satellites.⁴ Furthermore, it is involved in the chemistry of hot molecular cores and the outflow of dying carbon stars.⁵ Also, the reactions of CN radicals with unsaturated hydrocarbons are important steps in the production of long chain nitrile species.⁴ Because hydrogen cyanide is a common intermediate in hydrocarbon flames containing a nitrogen source, the CN radical is also particularly relevant to the combustion of hydrocarbons.⁶ The cyano radical often reacts via hydrogen abstraction with small, closed-shell molecules also found in interstellar and combustion environments.^{1,7} The reaction of CN radical with H₂ to form HCN and the subsequent reaction between HCN and atomic oxygen to form NO is an important aspect of NO formation from atmospheric nitrogen and nitrogen-containing fuels.^{8,9} Additionally, the cyano radical is a by-product of the decomposition of nitrogen oxide compounds.⁷ The production of HCN via the abstraction of H₂ by the cyano radical has been observed at very low temperatures, such as those in the ISM.¹⁰ Other hydrogen abstractions by the cyano radical, such as CN• + CH₄ → HCN + CH₃, are among the proposed reactions that take place in Titan's atmosphere³ and HCN is an impor-

tant intermediate in combustion environments and can be produced through cyano radical hydrogen abstractions. Accurately determining the energetics and rate constants of these reactions can provide insight into what is taking place in both combustion environments and the ISM.

In these hydrogen abstractions, either the carbon or nitrogen can abstract the hydrogen to form either HCN or HNC. HCN is an important intermediate in the combustion of hydrocarbons, but the isomer HNC has a lower stability and is rare on earth.¹¹ The abundance ratio of these two molecules in space is quite different. HNC has been observed to be as abundant as HCN, and in some cases moreso. The HNC/HCN abundance ratio has even been observed to be 1.55 in cold clouds with temperatures as low as 10 K.^{11,12} While the carbon terminal is more reactive, reactions with the nitrogen end are still feasible and have been considered in previous studies.^{1,13-17} Therefore, reactions with the nitrogen end will be examined as well. In this work, the following hydrogen abstraction reactions of the cyano radical with various small closed-shell molecules will be investigated using high-level *ab-initio* methods:



where X=H, CH₃, NH₂, OH, F, SiH₃, PH₂, SH, Cl, C₂H, and CN. In this study, we are primarily concerned with the energetics of the stationary points and kinetics of these reactions. Our primary goal with this work is to achieve accurate barrier heights which paint a picture of the potential energy surfaces of each reaction pathway. After accurately determining the barrier heights for these reactions, we can produce reliable rate constants over a wide range of temperatures which mimic the conditions in which these reactions occur. These highly accurate results may then be used by

^a Center for Computational Quantum Chemistry, University of Georgia, 140 Cedar Street, Athens, Georgia 30602, USA. E-mail: ccq@uga.edu

^b Department of Chemistry and Biochemistry, Taylor University, 236 W. Reade Avenue, Upland, Indiana 46989, USA.

[†] Electronic Supplementary Information (ESI) available: See DOI: 10.1039/cXCP00000x/

experimentalists when examining yet-uncharacterized reactions involving the cyano radical.

2 Methods

Equilibrium geometries of stationary points (both minima and transition states) were optimized using the CCSD(T)-F12a¹⁸ method with the aug-cc-pVTZ basis set¹⁹ in MOLPRO 2010.²⁰ Electronic energies of stationary points along all reactions were computed according to the focal point approach (FPA) of Allen and coworkers.^{21,22} Methods that describe electron correlation up to CCSDT(Q)²³ and basis sets as large as aug-cc-pV5Z¹⁹ were used in this study. CCSD(T)/aug-cc-pVXZ ($X = D, T, Q, 5$)²⁴ single point energies were computed using MOLPRO 2010²⁰ whereas the CCSDT/aug-cc-pVDZ and CCSDT(Q)/aug-cc-pVDZ corrections were obtained using MRCC 2018.²⁵ For third row elements (Si – Cl), aug-cc-pV($X+d$)Z ($X = D, T, Q, 5$)²⁴ basis sets were used to compute the CCSD(T) single point energies. As seen in Table 1, there is excellent convergence to the CBS limit and good convergence to the FCI limit. The CCSD(T) complete basis set (CBS) energies were obtained by extrapolating the Hartree–Fock energy and correlation energies using a three-point exponential equation²⁶ and a two-point inverse cubic equation,²⁷ respectively:

$$E_{\text{ref}}(X) = E_{\text{HF}}^{\infty} + ae^{-bX} \quad (1)$$

$$E_{\text{corr}}(X) = E_{\text{corr}}^{\infty} + aX^{-3} \quad (2)$$

The focal point energies were obtained with the following formula:

$$\Delta E_{\text{CCSDT(Q)/CBS}} = \Delta E_{\text{CCSD(T)/CBS}} + \delta E_{\text{T(Q)}} \quad (3)$$

Additional corrections were made to account for approximations made during the focal point computations. To account for the core-correlation neglected under the frozen-core approximation, the difference between the CCSD(T)/aug-cc-pCVQZ energies with and without core-electrons correlated was determined (δ_{CORE}). A scalar relativistic correction was obtained using X2C-CCSD(T)/aug-cc-pCVTZ-X2C (δ_{REL}).^{28,29} The clamped nuclei approximation was treated via diagonal Born–Oppenheimer corrections (δ_{DBOC})^{30,31} evaluated at the ROHF/aug-cc-pVTZ level of theory.¹⁹ Both the relativistic correction and the diagonal Born–Oppenheimer correction were carried out with CFOUR 2.0.³² An experimental shift (δ_{SO}) was included for the OH, F, Cl, and SH products to account for the splitting of the electronic ground state due to spin-orbit coupling.^{33,34} Finally, zero-point vibrational energies (δ_{ZPVE}) were obtained from the CCSD(T)-F12a/aug-cc-pVTZ harmonic vibrational frequencies. Anharmonic contributions for the zero-point vibrational energies of the reactants and products were also determined at the MP2/cc-pVDZ^{35–37} level of theory by applying VPT2^{38–43} using CFOUR 2.0.³² These corrections were included if they were considered significant (≥ 0.1 kcal mol⁻¹). These corrections were added together to obtain the relative enthalpy at 0K:

$$\Delta H_{0\text{K}} = \Delta E_{\text{CCSDT(Q)/CBS}} + \delta_{\text{CORE}} + \delta_{\text{REL}} + \delta_{\text{DBOC}} + \delta_{\text{ZPVE}} (+\delta_{\text{SO}}) \quad (4)$$

Rate constants were calculated over a range of temperatures

using canonical transition state theory:^{44,45}

$$k^{\text{TST}}(T) = \kappa(T) \frac{k_{\text{B}}T}{h} \frac{Q^{\text{TS}}(T)}{Q^{\text{R}}(T)} \exp\left(\frac{-\Delta H^{\ddagger}}{k_{\text{B}}T}\right) \quad (5)$$

where $Q^{\text{TS}}(T)$ and $Q^{\text{R}}(T)$ are the partition functions of the transition state (TS) and reactants (R) and ΔH^{\ddagger} is the barrier height for the reaction. The transmission coefficient, $\kappa(T)$, was determined with an asymmetric Eckart potential barrier given the relative enthalpies of the pre-reactive complex, transition state, and products for each reaction as well as the imaginary harmonic vibrational frequency corresponding to the reaction mode of the transition state.⁴⁶ Eckart tunneling was used because of its past success accurately describing the tunneling of hydrogen transfer reactions at moderate to high temperatures.^{47–50} The methods we are using are the most accurate in the 200 – 2000 K range. It is expected that contributions from the excited electronic states of CN will play a negligible role in the kinetics below 2000 K so it will not be investigated in this work. Additionally, pressure dependence was not accounted for in this work.

3 Results

3.1 Energies and Geometries

Tables 2 and 3 show the reaction enthalpies at 0 K for CN H-abstractions from the carbon and nitrogen terminals. As seen in the final two columns of each table, the agreement between our computed reaction enthalpies and the reaction enthalpies taken from the Active Thermochemical Tables (ATcT) (version 1.122e) is excellent.^{51–53} The latter results were unavailable for the reactions between CN and SiH₄, PH₃, and H₂S. All of our energy values for the carbon terminal abstractions lie within 0.20 kcal mol⁻¹ of the ATcT values, while those of the corresponding nitrogen abstractions lie within 0.30 kcal mol⁻¹. The mean absolute error of the carbon terminal abstraction reaction enthalpies is 0.09 kcal mol⁻¹ and 0.11 kcal mol⁻¹ for the nitrogen abstractions. The root mean square error for the carbon abstractions is 0.11 kcal mol⁻¹ and 0.14 kcal mol⁻¹ for the nitrogen abstractions. The largest deviation for both the carbon and nitrogen abstractions is that for HF, with differences of 0.20 kcal mol⁻¹ and 0.29 kcal mol⁻¹, respectively.

Table 4 shows the enthalpies of the carbon terminal abstraction transition states relative to their respective reactants. According to the results in Table 2, we may expect these barrier heights to be accurate within an uncertainty of 0.20 kcal mol⁻¹. The transition states with NH₃, PH₃, and H₂S have submerged barriers below the relative enthalpies of their respective reactants. This suggests that these reactions will be fast even at low temperatures. On the other hand, reactions with HF, C₂H₂, HCN, and HNC have barriers larger than 10 kcal mol⁻¹ so it is unlikely that these reactions will take place at room temperature. Reactions with H₂, CH₄, H₂O, HCl, and SiH₄ have barriers between 0 and 8 kcal mol⁻¹ so these reactions will proceed at a modest but non-negligible rate at moderate temperatures. For the reactions with moderate barriers, it is important to determine the barrier height to a high-level of accuracy in order to elucidate exactly how fast each reaction will occur.

Table 1 Representative focal point analysis table for the barrier height of the CN + H₂ reaction. Additional focal point tables can be found in the supplementary information

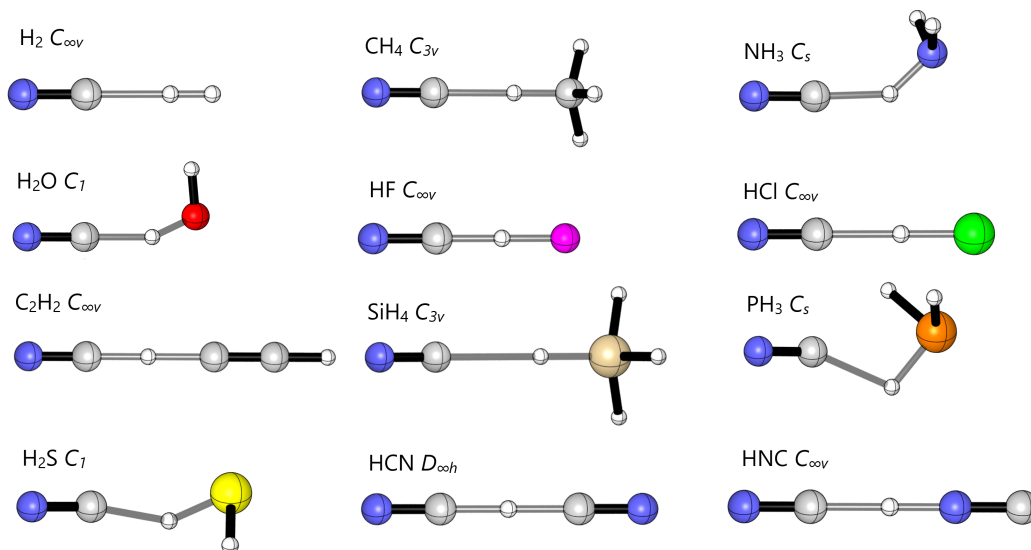
Basis Set	HF	+ δ MP2	+ δ CCSD	+ δ (T)	+ δ T	+ δ (Q)	Net
aug-cc-pVDZ	+12.48	-11.10	+2.86	-0.77	+0.22	-0.13	[+3.56]
aug-cc-pVTZ	+13.46	-11.57	+3.06	-0.84	[+0.22]	[-0.13]	[+4.20]
aug-cc-pVQZ	+13.69	-11.64	+3.10	-0.85	[+0.22]	[-0.13]	[+4.38]
aug-cc-pV5Z	+13.72	-11.62	+3.10	-0.85	[+0.22]	[-0.13]	[+4.45]
CBS Limit	[+13.72]	[-11.59]	[+3.11]	[-0.84]	[+0.22]	[-0.13]	[+4.49]

Table 2 Enthalpies at 0K (ΔH_{0K}) in kcal mol⁻¹ for products relative to reactants (CN + HX → HCN + X)

Donor	CBS ^a	$\delta_{T(Q)}$	δ_{CORE}	δ_{REL}	δ_{DBOC}	δ_{ZPVE}^b	δ_{SO}	Total	ATcT ^c
H ₂	-22.64	0.65	-0.52	0.07	0.00	0.78		-21.66	-21.76
CH ₄	-19.78	0.65	-0.34	0.05	0.00	-2.35(0.93)		-21.77	-21.66
NH ₃	-16.92	0.64	-0.22	-0.03	0.09	-2.52(0.18)		-18.95	-19.02
H ₂ O	-6.50	0.72	-0.30	-0.07	0.02	-1.06(0.16)	-0.20	-7.38	-7.38
HF	9.32	0.81	-0.34	-0.14	0.03	1.15	-0.39	10.44	10.24
SiH ₄	-35.55	0.63	-0.36	-0.06	-0.04	0.77		-34.60	
PH ₃	-44.54	0.67	-0.36	-1.63	-0.01	0.43		-45.44	
H ₂ S	-36.08	0.68	-0.32	-1.93	-0.01	-2.46	-0.54	-40.11	
HCl	-24.63	0.70	-0.29	-0.47	0.00	2.79	-0.84	-22.74	-22.82
C ₂ H ₂	7.12	0.38	-0.18	-0.07	0.02	-0.72		6.56	6.69
HNC	-14.91	-0.17	-0.20	-0.03	0.07	0.32		-14.93	-14.89

^aCBS denotes the CCSD(T)/CBS relative energy^bZero-point vibrational energies computed with the harmonic oscillator treatment, contributions from anharmonic treatment of the ZPVEs at the MP2/cc-pVDZ level of theory are in parentheses^cData taken from the Active Thermochemical Tables (ATcT)⁵¹⁻⁵³**Table 3** Enthalpies at 0K (ΔH_{0K}) in kcal mol⁻¹ for products relative to reactants (CN + HX → HNC + X)

Donor	CBS ^a	$\delta_{T(Q)}$	δ_{CORE}	δ_{REL}	δ_{DBOC}	δ_{ZPVE}^b	δ_{SO}	Total	ATcT ^c
H ₂	-7.73	0.82	-0.32	0.11	-0.10	0.46		-6.76	-6.86
CH ₄	-4.87	0.82	-0.14	0.09	-0.02	-2.67(0.94)		-6.79	-6.77
NH ₃	-2.00	0.81	-0.02	0.01	0.07	-2.84(0.20)		-3.97	-4.13
H ₂ O	8.41	0.90	-0.10	-0.04	0.04	-1.38(0.18)	-0.20	7.64	7.51
HF	24.24	0.98	-0.14	-0.10	0.01	0.83	-0.39	25.43	25.14
SiH ₄	-20.64	0.80	-0.16	-0.03	-0.05	0.45		-19.62	
PH ₃	-29.63	0.84	-0.16	-1.60	-0.10	0.11(0.10)		-30.54	
H ₂ S	-21.16	0.85	-0.12	-1.89	-0.02	-2.78(0.10)	-0.54	-25.13	
HCl	-9.72	0.87	-0.09	-0.43	-0.03	2.47	-0.84	-7.77	-7.92
C ₂ H ₂	22.04	0.55	0.02	-0.03	0.01	-1.04		21.54	21.58
HCN	14.92	0.16	0.20	0.03	-0.10	-0.32		14.93	14.89

^aCBS denotes the CCSD(T)/CBS relative energy^bZero-point vibrational energies computed with the harmonic oscillator treatment, contributions from anharmonic treatment of the ZPVEs at the MP2/cc-pVDZ level of theory are in parentheses^cData taken from the ATcT⁵¹⁻⁵³**Fig. 1** Geometries of R1 transition states.

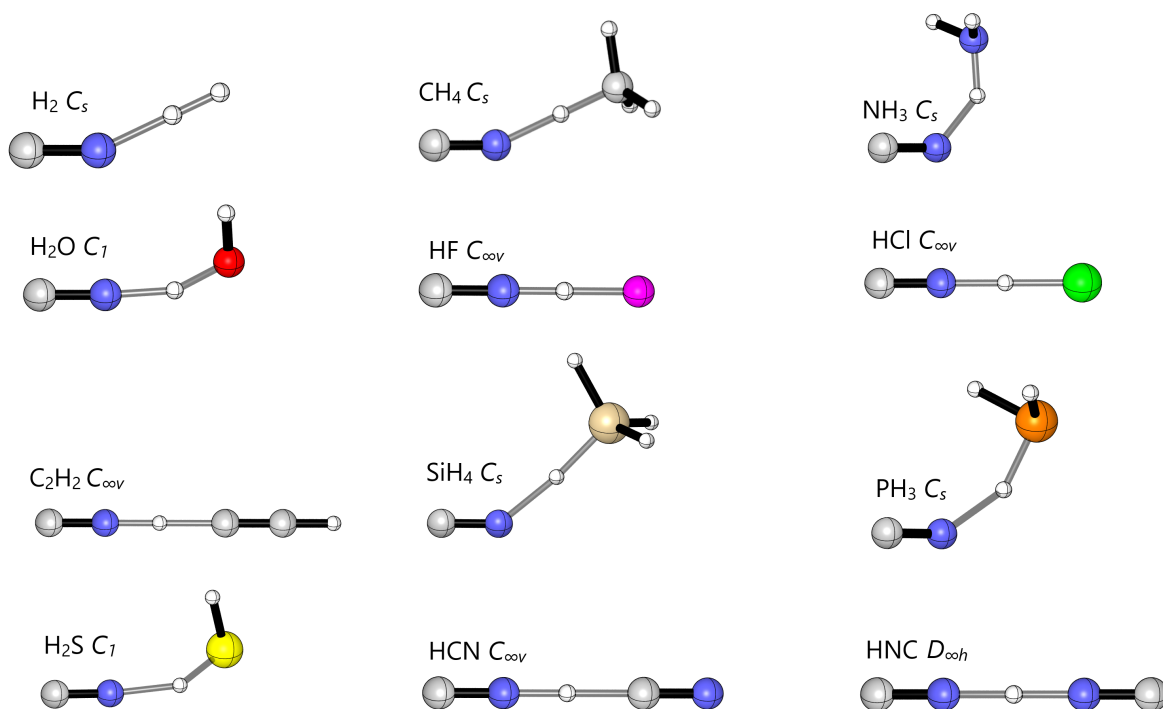


Fig. 2 Geometries of R2 transition states.

Table 4 Enthalpies in 0K in kcal mol⁻¹ of carbon terminal abstraction transition states relative to reactants (CN + HX → HCN + X)

Donor	CBS ^a	$\delta_{T(Q)}$	δ_{CORE}	δ_{REL}	δ_{DBOC}	δ_{ZPVE}	Total
H ₂	4.40	0.08	-0.02	0.03	0.11	-0.37	4.24
CH ₄	2.43	0.17	-0.06	-0.08	0.10	-1.37	1.19
NH ₃	-0.79	0.00	-0.11	-0.01	0.03	-1.53	-2.41
H ₂ O ^b	10.14	-0.55	-0.13	-0.05	0.16	-2.42	7.15
HF	24.67	-0.64	0.09	-0.09	0.02	-1.53	22.53
SiH ₄	-0.69	0.03	-0.04	0.02	0.01	1.02	0.35
PH ₃	-4.24	0.08	-0.15	0.36	0.01	0.35	-3.59
H ₂ S	-1.15	0.05	-0.17	0.33	0.10	0.09	-0.75
HCl	5.09	-0.01	-0.09	0.06	0.06	-1.64	3.47
C ₂ H ₂	18.64	0.20	-0.11	0.05	0.02	-3.55	15.25
HCN	18.47	0.00	0.02	0.00	0.15	-2.87	15.77
HNC	13.99	0.14	0.04	-0.08	0.02	-2.83	11.27

^aCBS denotes the CCSD(T)/CBS relative energy

^bThe transition state for the CN + H₂O → HCN + OH reaction was optimized at the CCSD(T)/aug-cc-pVTZ level of theory

Table 5 Enthalpies in 0K in kcal mol⁻¹ of nitrogen abstraction transition states relative to reactants (CN + HX → HNC + X)

Donor	CBS ^a	$\delta_{T(Q)}$	δ_{CORE}	δ_{REL}	δ_{DBOC}	δ_{ZPVE}	Total
H ₂	17.69	-0.28	0.04	0.01	0.38	-1.25	16.59
CH ₄	16.02	-0.20	0.13	0.04	0.06	-3.26	12.79
NH ₃	8.91	0.00	0.04	-0.01	0.01	-1.68	7.27
H ₂ O	21.59	-1.69	-0.09	-0.05	0.01	-2.86	16.91
HF	32.72	-0.94	-0.03	-0.08	-0.01	-3.40	28.25
SiH ₄	8.57	-0.22	-0.01	-0.04	0.15	-2.09	6.36
PH ₃	4.90	0.04	0.06	0.33	0.25	-1.33	4.25
H ₂ S	9.03	-0.76	-0.04	0.67	0.03	-1.45	7.47
HCl	11.60	-0.41	0.07	-0.15	0.09	-1.73	9.47
C ₂ H ₂	32.76	-0.17	0.07	-0.04	-0.01	-4.71	27.91
HCN	28.90	0.31	0.04	-0.08	0.02	-2.81	26.37
HNC	16.13	-0.33	0.06	0.00	0.07	-2.08	13.85

^aCBS denotes the CCSD(T)/CBS relative energy

Table 5 shows the nitrogen terminal abstraction transition state reaction enthalpies relative to their respective reactants. According to the results in Table 3, we may expect these barrier heights to be reliable within an uncertainty of $0.3 \text{ kcal mol}^{-1}$. None of the nitrogen terminal abstractions studied have submerged barriers, and in every case the transition state barriers for these abstractions are higher than those of the corresponding carbon terminal abstractions. The nitrogen terminal abstractions with H_2 , CH_4 , H_2O , HF , C_2H_2 , HCN , and HNC all have barriers greater than 10 kcal mol^{-1} and in some cases the barriers are greater than 20 kcal mol^{-1} . Because of this, these reactions are unlikely to take place at most temperatures. The remaining reactions, NH_3 , HCl , SiH_4 , PH_3 , and H_2S , have barriers less than 10 kcal mol^{-1} . These reactions are more likely to take place than the others; but in most cases the carbon terminal abstraction will dominate. Figure 3 depicts a visual representation of the barrier heights and relative enthalpies of the various hydrogen abstractions investigated in this research.

The δ_{T} and $\delta_{\text{(Q)}}$ corrections ($\delta_{\text{T(Q)}} = \delta_{\text{T}} + \delta_{\text{(Q)}}$) suggest that the energies reported in Tables 2, 3, 4, and 5 generally converge well to the FCI limit. Of the corrections reported in Tables 4 and 5, δ_{ZPVE} is the largest, suggesting that accurate barrier heights require accurate electronic energies as well as reliable vibrational frequencies. As expected, δ_{REL} is larger for the third row donors PH_3 , H_2S , and HCl . The diagonal Born–Oppenheimer corrections for the reaction enthalpies in Tables 2 and 3 were consistently small ($\leq 0.1 \text{ kcal mol}^{-1}$) while for the transition state barriers this is not the case, where δ_{DBOC} values are as large as $0.4 \text{ kcal mol}^{-1}$. The latter value is artifactual, almost surely due to a conical intersection involving the $\text{A } ^2\Pi$ state of the CN radical.

The isomerization energy barrier for $\text{HNC} \rightarrow \text{HCN}$ has been extensively studied in previous theoretical studies.^{54–64} In this work, it was predicted to be $44.61 \text{ kcal mol}^{-1}$, which is in agreement with the energy value range of $44.5 - 48.2 \text{ kcal mol}^{-1}$ reported by previous studies.^{54,56–59,63} This large energy barrier makes it unlikely that the HCN formed will isomerize into HNC at low temperatures. It will become more likely at higher temperatures, but we did not consider this in the present research.

3.2 Comparison between Hydrogen Abstractions by C_2H and CN

The ethynyl radical (C_2H) is another radical present in the interstellar medium and combustion environments. It is isoelectronic with the cyano radical and also has a high affinity for hydrogen abstraction from small closed-shell molecules. The transition state barrier enthalpies in Figure 4 were taken from a recent paper studying many of the same reactions with ethynyl radical as the abstraction agent instead.⁶⁵ This work on the ethynyl radical employed a very similar level of theory which allows us to make accurate direct comparisons. The transition state barriers of the cyano radical nitrogen terminal abstractions are significantly larger than the corresponding barriers for both the cyano radical carbon terminal abstractions and the ethynyl radical abstractions. Therefore, we have chosen to only draw comparisons between the ethynyl radical abstractions and the cyano radical carbon termi-

nal abstractions. When comparing reactions, we see that abstractions of NH_3 , PH_3 , and H_2S by the ethynyl radical and the cyano radical all have submerged barriers. In every case except for the abstractions of NH_3 and PH_3 , the barrier of the cyano radical carbon abstraction is higher than the analogous ethynyl barrier. The difference between the barrier heights of the ethynyl radical and cyano radical is less than 5 kcal mol^{-1} for all reactions except for the abstraction of HF and HCN . Therein the cyano radical abstraction of HF has a barrier height $8.80 \text{ kcal mol}^{-1}$ higher than that of the ethynyl radical, and the cyano radical abstraction of HCN has a barrier height $7.05 \text{ kcal mol}^{-1}$ higher than the corresponding ethynyl barrier.

3.3 Kinetics

Thus far, only the kinetics for the reactions resulting in the production of HCN have been studied. As discussed previously, in nearly every case, the reaction resulting in the production of HCN will be significantly faster than the corresponding reaction producing HNC. For this reason we chose to only report rate constants for a subset of reactions. Table 6 contains the rate constants for $\text{CN} + \text{H}_2$, H_2O , HCl , and SiH_4 using the rigid-rotor harmonic oscillator approximation. The reactions of $\text{CN} + \text{NH}_3$, PH_3 , and H_2S have submerged barriers, and as such the rate constants for these reactions at all temperatures will be large as most collisions result in the products NH_2 , PH_2 , and HS . On the other hand, the abstractions from C_2H_2 , HCN , HNC , and HF encounter barriers in excess of 10 kcal mol^{-1} and are not expected to be very important at most temperatures. Because of these considerations, we have only examined the rate constants for the abstractions from H_2 , CH_4 , H_2O , HCl , and SiH_4 . Table 6 displays the rate constants for the $\text{CN} + \text{H}_2$, CH_4 , H_2O , HCl , and SiH_4 reactions.

3.4 $\text{CN} + \text{H}_2$

Due to the simplicity of this system and its importance in interstellar and combustion chemistry, $\text{CN} + \text{H}_2 \rightarrow \text{HCN} + \text{H}$ has been extensively studied in numerous previous experimental^{66–71} and theoretical studies.^{16,55,72–81} Figure 5 shows features of the potential energy surface we obtained for this reaction. The reaction proceeds through a linear transition state at $4.24 \text{ kcal mol}^{-1}$ and then continues to the products at $-21.66 \text{ kcal mol}^{-1}$. Further results for this reaction as studied in this work can be found in the supplemental information.[†] Comparisons may be drawn between the theoretical results presented in this work and previous theoretical studies of this reaction; see Table 7. In Table 7, our results may be considered as the current highest level of theory incorporating a robust geometry as well as various incremental corrections to the electronic energy. The CAS+1+2+QC(3E,3O)/cc-pVTZ results from ter Horst et al.,¹⁶ the HFB/6-311G(2d,2p) results from Carvalho-Silva et al.,⁷⁴ and the MR-CI,3E,3O-CAS+1+2/cc-pVTZ results from He et al.⁷⁸ all agree reasonably well with our results. The barrier heights from these studies fall within $0.20 \text{ kcal mol}^{-1}$ of the barrier height we found in this study.

Table 6 contains the rate constants obtained for the reaction $\text{CN} + \text{H}_2 \rightarrow \text{HCN} + \text{H}$. Rate constants were obtained using

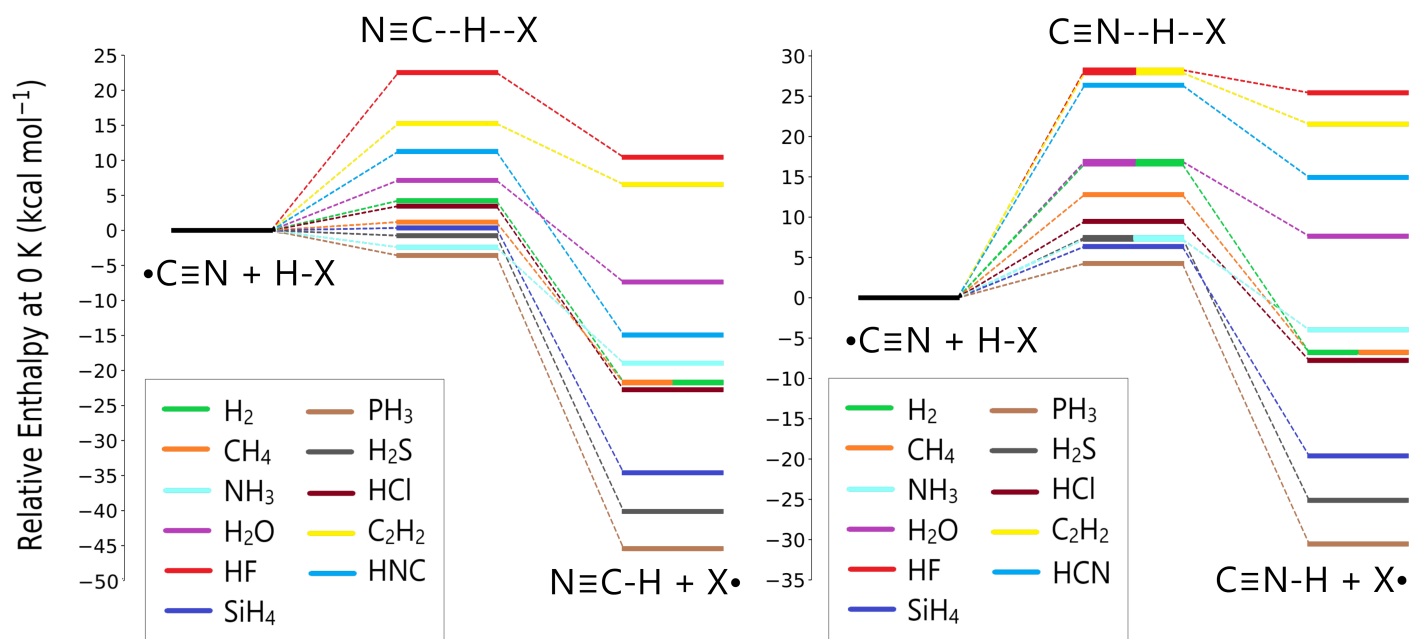


Fig. 3 Potential energy surfaces of all of the various hydrogen abstractions investigated in this work.

Table 6 Rate constants for $\text{CN} + \text{HX} \rightarrow \text{HCN} + \text{X}$ abstractions in $\text{cm}^3 \text{ molecule}^{-1} \text{ s}^{-1}$. Rate constants are obtained with the harmonic oscillator approximation unless stated otherwise

T/K	H ₂	CH ₄ ^a	H ₂ O	HCl	SiH ₄
50	3.61×10^{-19}	1.34×10^{-17}	8.36×10^{-19}	5.03×10^{-21}	2.68×10^{-13}
100	7.25×10^{-18}	2.71×10^{-14}	1.13×10^{-18}	5.87×10^{-19}	2.52×10^{-13}
150	1.26×10^{-16}	1.33×10^{-13}	2.50×10^{-18}	3.21×10^{-17}	2.81×10^{-13}
175	4.30×10^{-16}	2.29×10^{-13}	4.14×10^{-18}	1.31×10^{-16}	2.99×10^{-13}
200	1.24×10^{-15}	3.57×10^{-13}	7.20×10^{-18}	4.05×10^{-16}	3.17×10^{-13}
225	3.03×10^{-15}	5.21×10^{-13}	1.29×10^{-17}	1.03×10^{-15}	3.37×10^{-13}
250	6.54×10^{-15}	7.21×10^{-13}	2.34×10^{-17}	2.25×10^{-15}	3.57×10^{-13}
275	1.27×10^{-14}	9.59×10^{-13}	4.22×10^{-17}	4.38×10^{-15}	3.77×10^{-13}
295	2.03×10^{-14}	1.18×10^{-12}	6.99×10^{-17}	7.01×10^{-15}	3.93×10^{-13}
298	2.17×10^{-14}	1.21×10^{-12}	7.15×10^{-17}	7.49×10^{-15}	3.95×10^{-13}
300	2.27×10^{-14}	1.24×10^{-12}	7.48×10^{-17}	7.83×10^{-15}	3.97×10^{-13}
325	3.78×10^{-14}	1.56×10^{-12}	1.29×10^{-16}	1.30×10^{-14}	4.17×10^{-13}
350	5.95×10^{-14}	1.92×10^{-12}	2.16×10^{-16}	2.05×10^{-14}	4.38×10^{-13}
375	8.95×10^{-14}	2.33×10^{-12}	3.49×10^{-16}	3.08×10^{-14}	4.58×10^{-13}
400	1.29×10^{-13}	2.79×10^{-12}	5.47×10^{-16}	4.44×10^{-14}	4.78×10^{-13}
500	4.23×10^{-13}	5.11×10^{-12}	2.50×10^{-15}	1.46×10^{-13}	5.59×10^{-13}
1000	8.71×10^{-12}	3.20×10^{-11}	1.55×10^{-13}	3.36×10^{-12}	9.20×10^{-13}
1500	3.82×10^{-11}	9.25×10^{-11}	1.15×10^{-12}	1.63×10^{-11}	1.22×10^{-12}
2000	1.01×10^{-10}	1.93×10^{-10}	4.15×10^{-12}	4.57×10^{-11}	1.48×10^{-12}
3000	3.69×10^{-10}	5.30×10^{-10}	2.12×10^{-11}	1.78×10^{-10}	1.91×10^{-12}
4000	8.84×10^{-10}	1.05×10^{-9}	6.05×10^{-11}	4.38×10^{-10}	2.27×10^{-12}
5000	1.70×10^{-9}	1.77×10^{-9}	1.30×10^{-10}	8.58×10^{-10}	2.59×10^{-12}

^aC–H–C bending motion treated as an anharmonic vibration

Table 7 Comparison of the $\text{CN}(^2\Sigma^+) + \text{H}_2 \rightarrow \text{HCN} + \text{H}$ abstraction at various levels of theory. Enthalpies are given in kcal mol^{-1} , bond distances and angles of the transition state are given in Angstroms and degrees, respectively, and frequencies in cm^{-1}

Method	ΔH^\ddagger	ΔH_r	R_{CH}	ω^\ddagger
CCSDT(Q)/CBS//CCSD(T)-F12a/aug-cc-pVTZ ^a	4.24	-21.66	1.593	750i
QCISD(T)/6-311++G**//B3LYP/6-311++G** ^b	1.43	-20.18		
CAS+1+2+QC(3E,3O)/cc-pVTZ ^c	4.3	-20.0	1.62	684i
MRCl/cc-pVQZ ^d	3.49	-20.46		690i
HFB/6-311G(2d,2p) ^e	4.41			596i
MP2/6-311G(2d,2p) ^e	3.19			572i
MR-Cl,3E,3O-CAS+1+2/cc-pVTZ ^f	4.44		1.685	644i
G3 ^g	3.85	-22.83	1.701	1415i
Active Thermochemical Tables		-21.76		

^aThis work ^bZhao et al.⁸⁰ ^cter Horst et al.¹⁶ (QC here means a Davidson correction has been included) ^dJu et al.⁷⁹ ^eCarvalho-Silva et al.⁷⁴ ^fHe et al.⁷⁸ ^gAlbernaz and Barreto⁷³

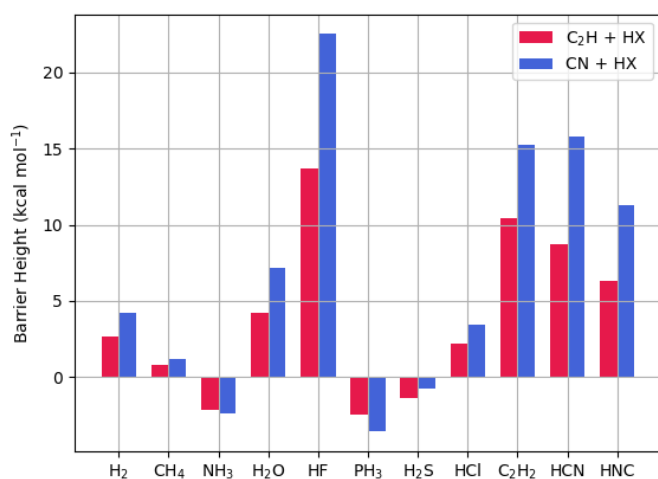


Fig. 4 Comparison of enthalpies at 0 K in kcal mol^{-1} of the $\text{C}_2\text{H} + \text{HX} \rightarrow \text{C}_2\text{H}_2 + \text{X}$ transition states, optimized at the CCSD(T)-F12a/aug-cc-pVTZ-F12 level of theory, and the $\text{CN} + \text{HX} \rightarrow \text{HCN} + \text{X}$ transition states, optimized at the CCSD(T)-F12a/aug-cc-pVTZ level of theory, relative to their respective reactants. Barrier height (ΔH^\ddagger) values can be found in Table 4 herein and in the study by Bowman and coworkers.⁶⁵

canonical transition state theory with Eckart tunneling corrections.^{44,45,47} Furthermore, to account for the uncertainty in the barrier height, we evaluated rate constants with transition state barriers $0.3 \text{ kcal mol}^{-1}$ higher and lower than the barrier height of $4.24 \text{ kcal mol}^{-1}$ that we reported. The rate constants with the increased barrier height of $4.54 \text{ kcal mol}^{-1}$ seem to match experiment the best in the range $300 - 700 \text{ K}$, while the rate constants obtained with the decreased barrier of $3.94 \text{ kcal mol}^{-1}$ overestimate the experimental rate constants over the $100 - 1000 \text{ K}$ range.

We compared our computed rate constants with previous theoretical and experimental works, as can be seen in Figure 6. Wagner and Bair⁷² computed their rate constants using conventional transition state theory with Wigner tunneling. They originally found a barrier height of $6.0 \text{ kcal mol}^{-1}$ (without zero-point vibrational correction) which they suspected was too high to be consistent with experimental rate constants. Instead, they reported rate constants using a barrier height of $4.1 \text{ kcal mol}^{-1}$, which repro-

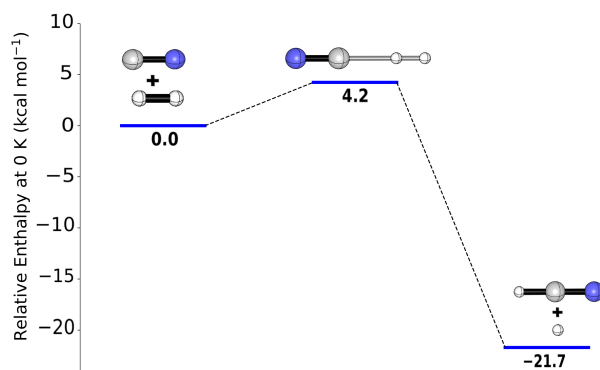


Fig. 5 Potential energy surface of the $\text{CN}(^2\Sigma^+) + \text{H}_2 \rightarrow \text{HCN} + \text{H}$ reaction at 0 K at the CCSDT(Q)/CBS//CCSD(T)-F12a/aug-cc-pVTZ level of theory. Internal coordinates for all structures can be found in the supplemental information.[†]

duced experimental rate constants.⁷² However, it appears their rate constants are a bit higher than experiment, suggesting their barrier height is not high enough. Albernaz and Barreto⁷³ obtained their rate constants using canonical variational transition state theory with Wigner tunneling. They reported a zero-point corrected barrier height for the reaction $\text{CN} + \text{H}_2 \rightarrow \text{HCN} + \text{H}$ of $3.85 \text{ kcal mol}^{-1}$ which is $0.39 \text{ kcal mol}^{-1}$ lower than the barrier found in this research.⁷³ This smaller barrier height along with the variational treatment of their rate constants likely lead to a slight underestimation of the experimental rate constants.

We also investigated the branching ratio for the reactions $\text{CN} + \text{H}_2 \rightarrow \text{HCN} + \text{H}$ and $\text{CN} + \text{H}_2 \rightarrow \text{HNC} + \text{H}$. The branching ratio between the formation of HNC versus HCN for these reactions is simply given as the ratio between canonical transition state theory rate constants between R2 and R1 for the H_2 donor at a certain temperature. At higher temperatures, the branching ratio becomes more evenly distributed between the production of HCN and HNC. In most cases, the barrier of the nitrogen terminal abstraction is at least 5 kcal mol^{-1} greater than the barrier of the corresponding carbon terminal abstraction. Therefore the production of HCN is expected to dominate the HNC production pathway at moderate to low temperatures.

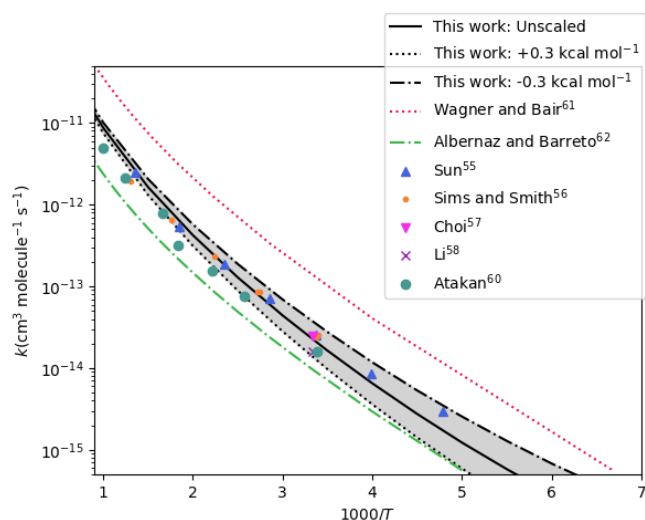


Fig. 6 Comparison between $\text{CN}(^2\Sigma^+) + \text{H}_2 \rightarrow \text{HCN} + \text{H}$ rate constants obtained in this work and previously reported experimental (markers)^{66–69,71} and theoretical rate constants (lines).^{72,73}

Albernaz and Barreto⁷³ also reported theoretical HNC/HCN branching ratios for the reaction $\text{CN} + \text{H}_2 \rightarrow \text{HNC}/\text{HCN} + \text{H}$. They predicted the branching ratio to be temperature dependent over the range 200 – 4000 K with the $\text{CN} + \text{H}_2 \rightarrow \text{HCN} + \text{H}$ reaction as the dominant channel. As the temperature increases to 4000 K, Albernaz found the HCN channel remains dominant with the probability > 99% in the range of temperatures they analyzed.⁷³ We found similar results for the branching ratio of this reaction, as may be seen in Figure 7. As the temperature increases from 40 K up to about 350 K, the HNC/HCN branching ratio quickly decreases to a minimum of less than 10^{-4} , suggesting that the $\text{CN} + \text{H}_2 \rightarrow \text{HNC} + \text{H}$ reaction channel is not as important at low temperatures. As the temperature increases past this point, the branching ratio begins to increase again, showing an increased favorability for the production of HNC. We agree with the findings of Albernaz and Barreto that the $\text{CN} + \text{H}_2 \rightarrow \text{HCN} + \text{H}$ pathway is the dominant reaction channel for this range of temperatures. However, as the temperature increases, the probability of this reaction channel decreases as the probability of the $\text{CN} + \text{H}_2 \rightarrow \text{HNC} + \text{H}$ increases.

3.5 $\text{CN} + \text{CH}_4$

The $\text{CN} + \text{CH}_4 \rightarrow \text{HCN} + \text{CH}_3$ reaction has also been studied in previous experimental^{17,66–69,71} and theoretical studies⁸² due to its importance in both combustion environments and the ISM. Figure 8 shows the stationary points we obtained for this reaction. This reaction proceeds through a transition state of C_{3v} symmetry with a small barrier height of $1.19 \text{ kcal mol}^{-1}$. The reaction then continues to the products HCN and CH_3 at $-21.77 \text{ kcal mol}^{-1}$. Further results for this reaction as studied in this work can be found in the supplemental information.[†] Rate constants for this reaction are provided in Table 6. In a previous study, we found that anharmonic treatments of low frequency vibrational modes may be necessary for highly accurate TST rate constants.⁶⁵ For

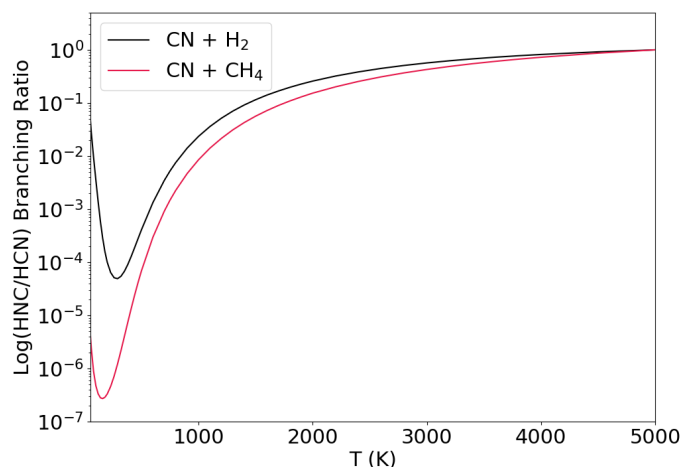


Fig. 7 Theoretical branching ratios for $\text{CN}(^2\Sigma^+) + \text{H}_2 \rightarrow \text{HNC}/\text{HCN} + \text{H}$ and $\text{CN}(^2\Sigma^+) + \text{CH}_4 \rightarrow \text{HNC}/\text{HCN} + \text{CH}_3(^2A'_2)$ as a function of temperature (40–5000 K) (this research).

the reaction $\text{CN} + \text{CH}_4 \rightarrow \text{HCN} + \text{CH}_3$ we also found this type of treatment to be necessary and it has been included. Our rate constants were obtained using canonical transition state theory with Eckart tunneling corrections using an anharmonic treatment of the first degenerate vibrational mode. Additionally, we computed rate constants for this reaction with barrier heights $0.3 \text{ kcal mol}^{-1}$ higher and lower than the barrier height we reported for this reaction. The rate constants computed with the reduced ($1.19 - 0.30$) barrier height of $0.89 \text{ kcal mol}^{-1}$ significantly overestimated the experimental rate constants, while the rate constants computed with the higher ($1.19 + 0.30$) barrier height of $1.49 \text{ kcal mol}^{-1}$ had excellent agreement with experimental rate constants in the range 100 – 500 K. The latter result is a bit surprising because higher levels of electronic structure theory (than those used here) tend to *decrease* barrier heights. However, our simple procedures for predicting the rate constants may be an important part of the disagreement between the 1.19 and $1.49 \text{ kcal mol}^{-1}$ barrier results.

We compared our computed rate constants with previous theoretical and experimental works, as shown in Figure 9. Espinosa-Garcia et al.⁸² computed their rate constants using canonical variational transition state theory (CVT) with multidimensional tunneling, and again with ring polymer molecular dynamics (RPMD). They computed their rate constants with a transition state barrier of $2.5 \text{ kcal mol}^{-1}$. Their CVT results seem to reproduce experimental data well in the range 300 – 1000 K while the RPMD seem to slightly overestimate the experimental rates in the same temperature range. Our results seem to match the experimental trend qualitatively, but our rate constants overestimate the experimental rates in this same temperature range. If we had used a variational treatment for our rate constants, it is possible they would have matched experiment better at high temperatures. At lower temperatures, the rate constants we computed with the barrier height $1.49 \text{ kcal mol}^{-1}$ have excellent agreement with experiment.

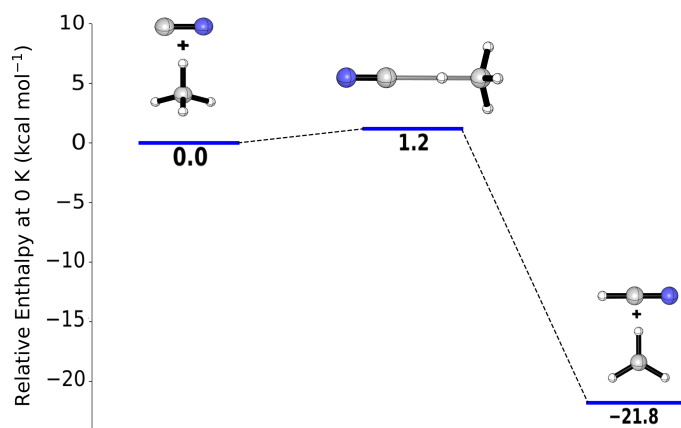


Fig. 8 Potential energy surface of $\text{CN}(^2\Sigma^+) + \text{CH}_4 \rightarrow \text{HCN} + \text{CH}_3(^2A_2')$ reaction at 0 K at the CCSDT(Q)/CBS//CCSD(T)-F12a/aug-cc-pVTZ level of theory. Internal coordinates for all structures can be found in the supplemental information.[†]

We investigated the branching ratio between the $\text{CN} + \text{CH}_4 \rightarrow \text{HCN} + \text{CH}_3$ and $\text{CN} + \text{CH}_4 \rightarrow \text{HNC} + \text{CH}_3$ reactions using the same methodology described before. Bethardy et al.⁸⁷ reported a HNC/HCN branching ratio for the reaction $\text{CN} + \text{CH}_4 \rightarrow \text{HNC}/\text{HCN} + \text{CH}_3$ of less than 10^{-4} at room temperature, which we have found to be true at low temperatures.⁸⁷ As the temperature increases from 40 K up to around 350 K, we found there is a decrease in the branching ratio, leading to a minimum of less than 10^{-6} at around room temperature. This value is in agreement with the results reported by Bethardy and coworkers. As the temperature increases past this point, the HNC/HCN branching ratio increases and approaches 1 as the temperature approaches 5000 K, showing that the reaction between $\text{CN} + \text{CH}_4$ may proceed over the $12.79 \text{ kcal mol}^{-1}$ barrier resulting in the production of $\text{HNC} + \text{CH}_3$. However, the $\text{CN} + \text{CH}_4 \rightarrow \text{HCN} + \text{CH}_3$ reaction will remain the dominant reaction pathway of the two. The relationship between branching ratio and temperature is illustrated in Figure 7, presented earlier.

3.6 $\text{CN} + \text{NH}_3$

The reaction $\text{CN} + \text{NH}_3 \rightarrow \text{HCN} + \text{NH}_2$ has a submerged barrier of $-2.41 \text{ kcal mol}^{-1}$, as seen in Figure 10. Because of this submerged barrier, rate constants for this reaction at all temperatures will be large, as most collisions will result in the products. The experiment of De Juan et al.⁸⁸ agrees with this. The rate constants they obtained for this reaction were so large that they concluded the absence of any significant potential barrier.⁸⁸ Other previous experimental and theoretical studies similarly found that this reaction has a rapid rate.^{14,89-91} Comparisons may be drawn between the theoretical results presented in this work and previous theoretical studies on this reaction, found in Table 8. Our results may be considered as the current highest level of theory incorporating a robust geometry as well as various incremental corrections to the electronic energy. The next highest level of

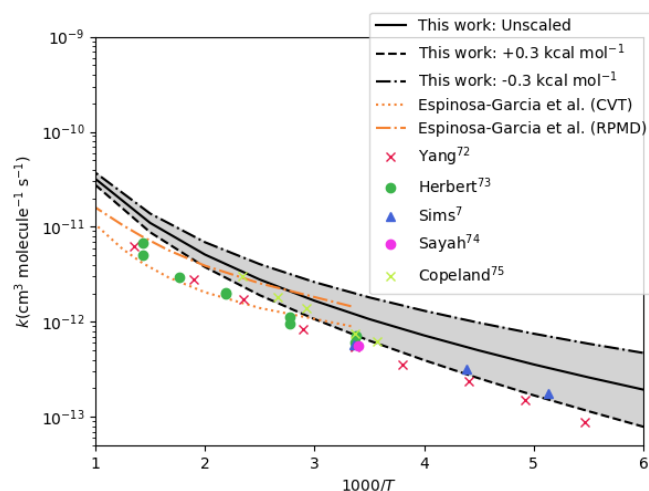


Fig. 9 Comparison between $\text{CN}(^2\Sigma^+) + \text{CH}_4 \rightarrow \text{HCN} + \text{CH}_3(^2A_2')$ rate constants obtained in this work and previously reported experimental (markers)^{7,83-86} and theoretical data (solid and dashed lines).⁸²

theory [CCSD(T)] is the work by Talbi and Smith found in Table 8.⁹² The transition state we found, shown in Figure 11, is in reasonable agreement with that which Talbi and Smith reported for the low energy pathway from $\text{CN} + \text{NH}_3$ to $\text{HCN} + \text{NH}_2$ using their potential energy surface. Our transition state barrier is $-2.41 \text{ kcal mol}^{-1}$, which is within $0.2 \text{ kcal mol}^{-1}$ of the transition state reported by Talbi and Smith.⁹² However, our exothermicity ($-18.95 \text{ kcal mol}^{-1}$) is in near perfect agreement with the ATcT result ($-19.02 \text{ kcal mol}^{-1}$) but quite distant from the earlier theoretical result ($-20.78 \text{ kcal mol}^{-1}$). Additionally, the geometric parameters of our transition state are in good agreement with those of Talbi and Smith, as can be seen in Table 8.

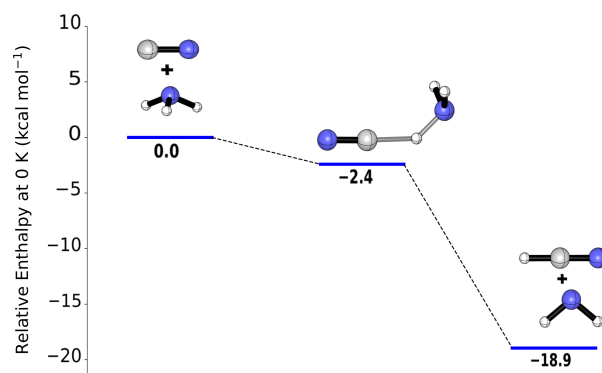
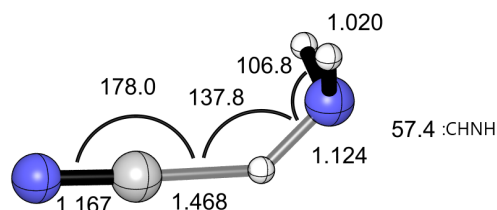


Fig. 10 Potential energy surface features for the $\text{CN}(^2\Sigma^+) + \text{NH}_3 \rightarrow \text{HCN} + \text{NH}_2(^2B_1)$ reaction at 0 K at the CCSDT(Q)/CBS//CCSD(T)/aug-cc-pVTZ level of theory. Internal coordinates for all structures can be found in the supplemental information.[†]

Table 8 Comparison of $\text{CN}(\Sigma^+) + \text{NH}_3 \rightarrow \text{HCN} + \text{NH}_2(^2B_1)$ abstraction at various levels of theory. Enthalpies are given in kcal mol^{-1} , bond distances and angles of the transition state are given in Angstroms and degrees, respectively, and frequencies in cm^{-1}

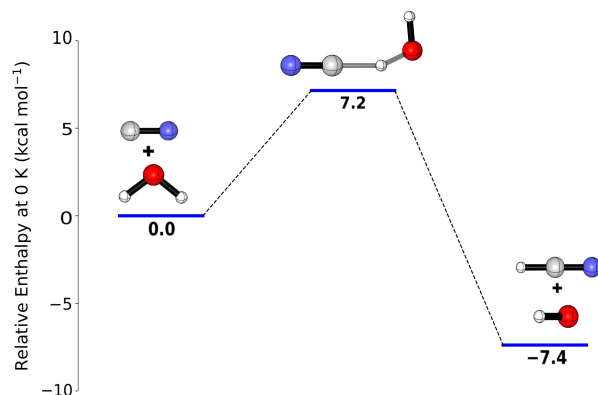
Theory	ΔH^\ddagger	ΔH_f	R_{CH}	R_{NH}	$\angle \text{CHN}$	ω^\ddagger
CCSDT(Q)/CBS//CCSD(T)-F12a/aug-cc-pVTZ ^a	-2.41	-18.95	1.46	1.12	137.8°	1068i
CCSD(T)/6-311+G(3df,2pd)//CCSD/6-311G(d,p) ^b	-2.60	-20.78	1.54	1.09	133.9°	846i
Active Thermochemical Tables		-19.02				

^aThis work^bTalbi and Smith⁹²**Fig. 11** C_s symmetric $\text{CN}(\Sigma^+) + \text{NH}_3$ transition state found in this work optimized at the CCSD(T)-F12a/aug-cc-pVTZ level of theory. Bond angles and bond distances are given in degrees and in angstroms, respectively.

3.7 CN + H₂O

Due to its importance in the ISM and combustion environments, the $\text{CN} + \text{H}_2\text{O} \rightarrow \text{HCN} + \text{OH}$ reaction has been studied in previous experimental^{93–95} and theoretical studies.⁹⁶ Figure 12 shows the stationary point energies we obtained for this reaction. This reaction proceeds through a transition state of C_1 symmetry with a barrier height of $7.15 \text{ kcal mol}^{-1}$. The reaction then proceeds to the products HCN and OH at $-7.38 \text{ kcal mol}^{-1}$. Further results for this reaction as studied in this work can be found in the supplemental information.[†] The δ_T and $\delta_{(Q)}$ corrections for this transition state were found to be 0.12 and $-0.67 \text{ kcal mol}^{-1}$, respectively, suggesting that further corrections may be necessary to better converge the focal point energy to the FCI limit. Rate constants for this reaction can be found in Table 6. Our rate constants were obtained using canonical transition state theory with Eckart tunneling corrections. Additionally, we computed rate constants for this reaction with a barrier height $0.3 \text{ kcal mol}^{-1}$ higher and lower than the barrier height we reported for this reaction. The rate constants computed with both modified barrier heights and those computed with our actual barrier height of $7.15 \text{ kcal mol}^{-1}$ fall between the two sets of experimental results, seen in Figure 13.

We compared our computed rate constants with previous theoretical and experimental studies, as illustrated in Figure 13. Wang et al.⁹⁶ computed their rate constants using both conventional transition state theory and canonical variational transition state theory (CVT). They further corrected their CVT rate constants with small-curvature tunneling (SCT).⁹⁶ They optimized their stationary points for this reaction at the QCISD(T)/6-311+G(2df,2p)//QCISD/6-311G(d,p) level of theory. They reported a transition state barrier height of $7.51 \text{ kcal mol}^{-1}$ with zero-point energy included. Based on their results, Wang et al. concluded that the variational effect is very small in the calculation of the rate constants. They also concluded that the SCT

**Fig. 12** Potential energy surface features for the $\text{CN}(\Sigma^+) + \text{H}_2\text{O} \rightarrow \text{HCN} + \text{OH}(\Sigma^+)$ reaction at 0 K at the CCSDT(Q)/CBS//CCSD(T)/aug-cc-pVTZ level of theory. Internal coordinates for all structures can be found in the supplemental information.[†]

corrections were necessary, so they consider their CVT/SCT results to be the most reliable.⁹⁶ The TST results they reported fall between the experimental results while their CVT/SCT results fall slightly above the experimental results reported by Jacobs et al.⁹³ Our results seem to match the experimental trend well qualitatively, falling between the experimental rate constants reported by Jacobs et al. and Szekely et al.^{93,95} We also obtained rate constants with modified barrier heights $0.3 \text{ kcal mol}^{-1}$ higher and lower than our reported barrier height to explore whether our barrier was too high or too low. As can be seen in Figure 13, these modified barrier heights do not significantly alter our rate constants with respect to the experimental results. At high temperatures, our rate constants match well with the transition state theory results reported by Wang et al.⁹⁶ We obtained a transition state barrier for this reaction of $7.15 \text{ kcal mol}^{-1}$, which is slightly lower than their transition state barrier of $7.51 \text{ kcal mol}^{-1}$.⁹⁶ Future experimental studies of this reaction may be necessary. The two experimental studies compared in this work disagree significantly, and the theoretical results found in this study are not in excellent agreement with either set of experimental results.

4 Conclusions

The energetics of the cyano radical hydrogen abstractions of H_2 , CH_4 , NH_3 , H_2O , HF , SiH_4 , PH_3 , H_2S , HCl , C_2H_2 , HCN , and HNC with both the carbon and nitrogen terminals have been determined using highly accurate *ab initio* methods. We were able to achieve sub-chemical accuracy through a variety of additive energy corrections and we obtained excellent agreement with the

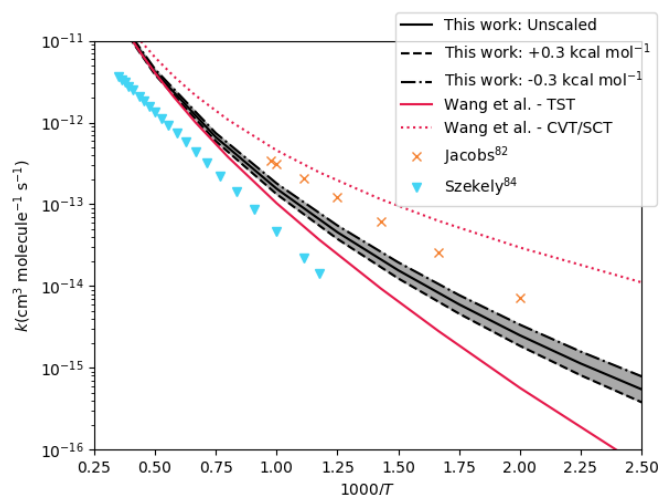


Fig. 13 Comparison between $\text{CN}(^2\Sigma^+) + \text{H}_2\text{O} \rightarrow \text{HCN} + \text{OH}(^2\Pi)$ rate constants obtained in this work and previously reported experimental (markers)^{93,95} and theoretical data (solid and dashed lines).⁹⁶

Active Thermochemical Table values. Accurate transition state barriers have been obtained for all reactions with the carbon and nitrogen terminals. It was found that the carbon terminal abstractions of NH_3 , PH_3 , and H_2S have submerged barriers below the relative enthalpies of their respective reactants. Abstractions of H_2 , CH_4 , H_2O , HCl , and SiH_4 have barriers between 0 and 8 kcal mol^{-1} . Abstractions of HF , C_2H_2 , HCN , and HNC have barriers larger than 10 kcal mol^{-1} . It was also found that the nitrogen terminal abstractions have higher barrier heights and are almost always slower than the analogous carbon terminal abstractions. The energetics for the nitrogen terminal abstractions presented in this research may aid any future experimental studies of these reactions. Accurate rate constants were obtained for the $\text{CN} + \text{H}_2/\text{CH}_4/\text{H}_2\text{O}/\text{HCl}/\text{SiH}_4 \rightarrow \text{HCN} + \text{H}/\text{CH}_3/\text{OH}/\text{Cl}/\text{SiH}_3$ reactions. Excellent agreement was demonstrated for the computed rate constants for the $\text{CN} + \text{H}_2 \rightarrow \text{HCN} + \text{H}$ reaction with current experimental rate constants without adjusting the barrier height. Good agreement for the computed rate constants for the $\text{CN} + \text{CH}_4 \rightarrow \text{HCN} + \text{CH}_3$ and $\text{CN} + \text{H}_2\text{O} \rightarrow \text{HCN} + \text{OH}$ reactions with current experimental rate constants was also demonstrated. Based on the agreement of these rate constants with experiment, the computed rate constants for the $\text{CN} + \text{HCl} \rightarrow \text{HCN} + \text{Cl}$ and $\text{CN} + \text{SiH}_4 \rightarrow \text{HCN} + \text{SiH}_3$ reactions are expected to be reliable. The $\text{CN} + \text{HCl} \rightarrow \text{HCN} + \text{Cl}$ reaction has not been as extensively studied as the $\text{CN} + \text{H}_2/\text{CH}_3/\text{H}_2\text{O} \rightarrow \text{H}/\text{CH}_3/\text{OH}$ reactions, and the $\text{CN} + \text{SiH}_4 \rightarrow \text{HCN} + \text{SiH}_3$ reaction has not yet been studied, so these results will be useful to guide future experimental and theoretical studies.

Conflicts of interest

There are no conflicts to declare.

Acknowledgements

The authors gratefully acknowledge support from the US Department of Energy (DOE), Office of Basic Energy Sciences (BES),

Computational and Theoretical Chemistry (CTC) Program, under Grant No. DE-SC0018412.

Notes and references

- 1 K. Gopalsamy, S. Thirupati and R. O. Ramabhadran, *ACS Earth Sp. Chem.*, 2019, **3**, 1080–1095.
- 2 A. McKellar, *Publ. Astron. Soc. Pac.*, 1940, **52**, 187–192.
- 3 D. W. Clarke and J. P. Ferris, *Orig. Life Evol. Biosph.*, 1997, **27**, 225–248.
- 4 K. Fukuzawa, Y. Osamura and H. F. Schaefer, *Astrophys. J.*, 1998, **505**, 278.
- 5 L. C. L. Huang, O. Asvany, A. H. H. Chang, N. Balucani, S. H. Lin, Y. T. Lee and R. I. Kaiser, *J. Chem. Phys.*, 2000, **113**, 8656.
- 6 R. A. Bair and T. H. Dunning Jr., *J. Chem. Phys.*, 1985, **82**, 2280–2294.
- 7 I. R. Sims, J. L. Queffelec, D. Travers, R. R. Bertrand, L. B. Herbert, J. Karthäuser and I. W. M. Smith, *Chem. Phys. Lett.*, 1993, **211**, 461–468.
- 8 S. T. Wooldridge, R. K. Hanson and C. T. Bowman, *Int. J. Chem. Kin.*, 1996, **28**, 245–258.
- 9 J. A. Miller and C. T. Bowman, *Prog. Energy Combust. Sci.*, 1989, **15**, 287–338.
- 10 F. Borget, S. Müller, D. Grote, P. Theulé, V. Vinogradoff, T. Chiavassa and W. Sander, *Astron. Astrophys.*, 2017, **598**.
- 11 D. Talbi, *Chem. Phys. Lett.*, 1999, **313**, 626–632.
- 12 W. M. Irvine and F. P. Schloerb, *Astrophys. J.*, 1984, **282**, 516–521.
- 13 E. Arunan, G. Manke II and D. W. Setser, *Chem. Phys. Lett.*, 1993, **207**, 81–87.
- 14 R. F. Meads, R. G. A. R. Maclagan and L. F. Phillips, *J. Chem. Phys.*, 1993, **97**, 3257–3265.
- 15 B. Atakan and J. Wolfrum, *Chem. Phys. Lett.*, 1991, **186**.
- 16 M. A. ter Horst, G. C. Schatz and L. B. Harding, *J. Chem. Phys.*, 1996, **105**, 558–571.
- 17 R. J. Balla, K. H. Casleton, J. S. Adams and L. Pasternack, *J. Phys. Chem.*, 1991, **95**, 8694–8701.
- 18 G. Knizia, T. B. Adler and H. J. Werner, *J. Chem. Phys.*, 2009, **130**, 054104.
- 19 E. Papajak, J. Zheng, X. Xu, H. R. Leverentz and D. G. Truhlar, *J. Chem. Theory Comput.*, 2011, **7**, 3027–3034.
- 20 H. J. Werner, P. J. Knowles, G. Knizia, F. R. Manby, M. Schütz, P. Celani, W. Györffy, D. Kats, T. Korona, R. Lindh, A. Mitrushenkov, G. Rauhut, K. R. Shamasundar, T. B. Adler, R. D. Amos, S. J. Bennie, A. Bernhardsson, A. Berning, D. L. Cooper, M. J. O. Deegan, A. J. Dobbyn, F. Eckert, E. Goll, C. Hampel, A. Hesselmann, G. Hetzer, T. Hrenar, G. Jansen, C. Köppl, S. J. R. Lee, Y. Liu, A. W. Lloyd, Q. Ma, R. A. Mata, A. J. May, S. J. McNicholas, W. Meyer, T. F. Miller III, M. E. Mura, A. Nicklass, D. P. O'Neill, P. Palmieri, D. Peng, K. Pflüger, R. Pitzer, M. Reiher, T. Shiozaki, H. Stoll, A. J. Stone, R. Tarroni, T. Thorsteinsson, M. Wang and M. Welborn, 2019, see <https://www.molpro.net>.
- 21 A. G. Császár, W. D. Allen and H. F. Schaefer III, *J. Chem. Phys.*, 1998, **108**, 9751–9764.

- 22 A. L. L. East and W. D. Allen, *J. Chem. Phys.*, 1993, **99**, 4638–4650.
- 23 Y. J. Bomble, J. F. Stanton, M. Kállay and J. Gauss, *J. Chem. Phys.*, 2005, **123**, 054101.
- 24 T. H. Dunning Jr., K. A. Peterson and A. K. Wilson, *J. Chem. Phys.*, 2001, **114**, 9244–9253.
- 25 M. Kállay, P. R. Nagy, D. Mester, Z. Rolik, G. Samu, J. Csontos, J. Csóka, P. B. Szabó, L. Gyevi-Nagy, B. Hégyel, I. Ladjánszki, L. Szegedy, B. Ladóczki, K. Petrov, M. Farkas, P. D. Mezei and Á. Ganyecz, *J. Chem. Phys.*, 2020, **152**, 074107.
- 26 D. Feller, *J. Chem. Phys.*, 1992, **96**, 6104–6114.
- 27 T. Helgaker, W. Klopper, H. Koch and J. Noga, *J. Chem. Phys.*, 1997, **106**, 9639–9646.
- 28 L. Cheng and J. Gauss, *J. Chem. Phys.*, 2011, **135**, 084114.
- 29 <http://slater.chemie.uni-mainz.de/cfour/index.php?n=Main.RecontractedCorrelation-consistentBasisFunctions> Accessed: 2020-05-06.
- 30 H. Sellers and P. Pulay, *Chem. Phys. Lett.*, 1984, **103**, 463–465.
- 31 N. C. Handy, Y. Yamaguchi and H. F. Schaefer III, *J. Chem. Phys.*, 1986, **84**, 4481–4484.
- 32 D. A. Matthews, L. Cheng, M. E. Harding, F. Lipparini, S. Stopkowitz, T. C. Jagau, P. G. Szalay, J. Gauss and J. F. Stanton, *J. Chem. Phys.*, 2020, **152**, 214108.
- 33 K. P. Huber and G. Herzberg, *Molecular Spectra and Molecular Structure: IV, Constants of Diatomic Molecules*, 2013.
- 34 C. E. Moore, *Atomic Energy Levels as Derived from the Analyses of Optical Spectra, Vol. 1*, 1949.
- 35 C. Møller and M. S. Plesset, *Phys. Rev.*, 1934, **46**, 618–622.
- 36 J. A. Pople, J. S. Binkley and R. Seeger, *Int. J. Quantum Chem., Symp.*, 1976, **10**, 1–19.
- 37 T. H. Dunning Jr., *J. Chem. Phys.*, 1989, **90**, 1007–1023.
- 38 H. H. Nielson, *Rev. Mod. Phys.*, 1951, **23**, 90–136.
- 39 J. K. G. Watson, in *Vibrational Spectra and Structure*, ed. J. R. Durig, Elsevier: Amsterdam, 1977, vol. 6, p. 1.
- 40 I. M. Mills, in *Molecular Spectroscopy: Modern Research*, ed. K. N. Rao and C. W. Matthew, Academic: New York, 1972, vol. 1, p. 115.
- 41 D. Papousek and M. R. Aliev, *Molecular Vibrational-Rotational Spectra*, Elsevier, Amsterdam, 1982.
- 42 D. A. Clabo Jr., W. D. Allen, R. B. Remington, Y. Yamaguchi and H. F. Schaefer III, *Chem. Phys.*, 1988, **123**, 187–239.
- 43 W. D. Allen, Y. Yamaguchi, A. G. Császár, D. A. Clabo Jr., R. B. Remington and H. F. Schaefer III, *Chem. Phys.*, 1990, **145**, 427–466.
- 44 H. Eyring, *J. Chem. Phys.*, 1935, **3**, 107–115.
- 45 D. G. Truhlar, B. C. Garrett and S. J. Klippenstein, *J. Phys. Chem.*, 1996, **100**, 12771–12800.
- 46 H. S. Johnston and J. Heicklen, *J. Phys. Chem.*, 1962, **66**, 532–533.
- 47 H. S. Johnston and J. Heicklen, *J. Phys. Chem.*, 1962, **66**, 532–533.
- 48 F. Zhang and T. S. Dibble, *Phys. Chem. Chem. Phys.*, 2011, **13**, 17969–17977.
- 49 B. Sirjean, E. Dames, H. Wang and W. Tsang, *J. Phys. Chem. A*, 2012, **116**, 319–332.
- 50 Y. Sha and T. S. Dibble, *J. Phys. Chem. A*, 2012, **116**, 319–332.
- 51 B. Ruscic, R. E. Pinzon, M. L. Morton, G. von Laszewski, S. J. Bittner, S. G. Nijsure, K. A. Amin, M. Minkoff and A. F. Wagner, *J. Phys. Chem. A*, 2004, **108**, 9979–9997.
- 52 B. Ruscic, R. E. Pinzon, G. von Laszewski, D. Kodeboyina, A. Burcat, D. Leahy, D. Montoy and A. F. Wagner, *J. Phys. Conf. Ser.*, 2005, **16**, 561–570.
- 53 B. Ruscic and D. H. Bross, 2019, <https://atct.anl.gov/>.
- 54 T. J. Lee and A. P. Rendell, *Chem. Phys. Lett.*, 1991, **177**, 491–497.
- 55 W. Quapp and A. Zech, *J. Comp. Chem.*, 2009, **31**, 573–585.
- 56 J. M. Bowman, B. Gazdy, J. A. Bentley, T. J. Lee and C. E. Dateo, *J. Chem. Phys.*, 1993, **99**, 308–323.
- 57 B. Gazdy, D. G. Musaev, J. M. Bowman and K. Morokuma, *Chem. Phys. Lett.*, 1995, **237**, 27–32.
- 58 D. Talbi and Y. Ellinger, *Chem. Phys. Lett.*, 1996, **263**, 385–392.
- 59 R. Contreras, V. S. Safont, P. Pérez, J. Andrés, V. Moliner and O. Tapia, *J. Mol. Struct.-Theochem.*, 1998, **426**, 277–288.
- 60 A. D. Isaacson, *J. Phys. Chem. A*, 2005, **110**, 379–388.
- 61 A. E. DePrince III and D. A. Mazziotti, *J. Phys. Chem. B*, 2008, **112**, 16158–16162.
- 62 S. Gutiérrez-Oliva, S. Díaz, A. Toro-Labbé, P. Lane, J. S. Murray and P. Politzer, *Mol. Phys.*, 2013, **112**, 349–354.
- 63 M. C. Lin, Y. He and C. F. Melius, *Int. J. Chem. Kin.*, 1992, **24**, 1103–1107.
- 64 P. K. Pearson, H. F. Schaefer and U. Wahlgren, *J. Chem. Phys.*, 1975, **62**, 350–354.
- 65 M. C. Bowman, A. D. Burke, J. M. Turney and H. F. Schaefer III, *Mol. Phys.*, 2020, **118**,.
- 66 Q. Sun, D. L. Yang, N. S. Wang, J. M. Bowman and M. C. Lin, *J. Chem. Phys.*, 1990, **93**, 4730–4739.
- 67 I. R. Sims and I. W. M. Smith, *Chem. Phys. Lett.*, 1988, **149**, 565–571.
- 68 N. Choi, M. A. Blitz, K. McKee, M. J. Pilling and P. W. Seakins, *Chem. Phys. Lett.*, 2004, **384**, 68–72.
- 69 X. Li, N. Sayah and W. M. Jackson, *J. Chem. Phys.*, 2004, **81**, 833–840.
- 70 G. He, I. Tokue and R. G. Macdonald, *J. Chem. Phys. A*, 1998, **102**, 4585–4591.
- 71 B. Atakan, A. Jacobs, M. Wahl, R. Weller and J. Wolfrum, *Chem. Phys. Lett.*, 1989, **154**, 449–453.
- 72 A. F. Wagner and R. A. Bair, *Int. J. Chem. Kin.*, 1986, **18**, 473–486.
- 73 A. F. Albernaz and P. R. P. Barreto, *Theor. Chem. Acc.*, 2019, **138**, 1–10.
- 74 V. H. Carvalho-Silva, V. Aquilanti, H. C. B. de Oliveira and K. C. Mundim, *J. Comp. Chem.*, 2017, **38**, 178–188.
- 75 C. Coletti and G. D. Billing, *J. Chem. Phys.*, 2000, **113**, 11101–11108.
- 76 D. H. Zhang and S. Y. Lee, *J. Chem. Phys.*, 2000, **112**, 203–

- 211.
- 77 A. L. Kaledin, M. C. Heaven and J. M. Bowman, *J. Chem. Phys.*, 1999, **110**, 10380–10392.
- 78 G. He, I. Tokue, L. B. Harding and R. G. Macdonald, *J. Phys. Chem. A.*, 1998, **102**, 7653–7661.
- 79 L. P. Ju, K. L. Han and J. Z. H. Zhang, *J. Theor. Comp. Chem.*, 2006, **5**, 769–777.
- 80 R. Zhao, D. Gao, X. Pan, L. Song, H. Yu, S. Yu and L. Yao, *Chem. Phys.*, 2019, **516**, 38–47.
- 81 B. S. Jursic, *J. Mol. Struct.-Theochem.*, 1998, **428**, 55–59.
- 82 J. Espinosa-Garcia, C. Rangel and Y. V. Suleimanov, *Phys. Chem. Chem. Phys.*, 2017, **19**, 19341–19351.
- 83 D. L. Yang, T. Yu, M. C. Lin and C. F. Melius, *Chem. Phys.*, 1993, **177**, 271–280.
- 84 L. Herbert, I. W. M. Smith and R. D. Spencer-Smith, *Int. J. Chem. Kin.*, 1992, **24**, 791–802.
- 85 N. Sayah, X. Li, J. F. Caballero and W. M. Jackson, *J. Photochem. Photobiol. A.*, 1988, **45**, 177–194.
- 86 L. R. Copeland, F. Mohammad, M. Zahedi, D. H. Volman and W. M. Jackson, *J. Chem. Phys.*, 1992, **96**, 5817–5826.
- 87 G. A. Bethardy, F. J. Northrup and R. G. Macdonald, *J. Chem. Phys.*, 1996, **105**, 4533–4549.
- 88 J. de Juan, I. W. M. Smith and B. Veyret, *J. Phys. Chem.*, 1987, **91**, 69–72.
- 89 I. R. Sims, J. L. Queffelec, A. Defrance, C. Rebrion-Rowe, D. Travers, P. Bocherel, B. R. Rowe and I. W. M. Smith, *J. Chem. Phys.*, 1994, **100**, 4229–4241.
- 90 A. Faure, C. Rist and P. Valiron, *Chem. Phys.*, 1999, **241**, 29–42.
- 91 A. Faure, C. Rist and P. Valiron, *Astron. Astrophys.*, 1999, **348**, 972–977.
- 92 D. Talbi and I. W. M. Smith, *Phys. Chem. Chem. Phys.*, 2009, **11**, 8477–8483.
- 93 A. Jacobs, M. Wahl, R. Weller and J. Wolfrum, *Chem. Phys. Lett.*, 1988, **144**, 203–207.
- 94 S. T. Wooldridge, R. K. Hanson and C. T. Bowman, *Int. J. Chem. Kin.*, 1995, **27**, 1075–1087.
- 95 A. Szekely, R. K. Hanson and C. T. Bowman, *Int. J. Chem. Kin.*, 1984, **16**, 1609–1621.
- 96 C. Y. Wang, S. Zhang and Q. S. Li, *Theo. Chem. Acc.*, 2002, **108**, 341–346.